Contents lists available at ScienceDirect

Nuclear Instruments and Methods in Physics Research A

journal homepage: www.elsevier.com/locate/nima

Time resolution deterioration with increasing crystal length in a TOF-PET system

S. Gundacker *, A. Knapitsch, E. Auffray, P. Jarron, T. Meyer, P. Lecoq

European Organization for Nuclear Research (CERN), 1211 Geneva 23, Switzerland

ARTICLE INFO

ABSTRACT

Highest time resolution in scintillator based detectors is becoming more and more important. In medical detector physics L(Y)SO scintillators are commonly used for time of flight positron emission tomography (TOF-PET). Coincidence time resolutions (CTRs) smaller than 100 ps FWHM are desirable in order to improve the image signal to noise ratio and thus give benefit to the patient by shorter scanning times. Also in high energy physics there is the demand to improve the timing capabilities of calorimeters down to 10 ps. To achieve these goals it is important to study the whole chain, i.e. the high energy particle interaction in the crystal, the scintillation process itself, the scintillation light transfer in the crystal, the photodetector and the electronics. Time resolution measurements for a PET like system are performed with the time-over-threshold method in a coincidence setup utilizing the ultra-fast amplifier-discriminator NINO. With $2 \times 2 \times 3 \text{ mm}^3$ LSO:Ce codoped 0.4%Ca crystals coupled to commercially available SiPMs (Hamamatsu S10931-050P MPPC) we achieve a CTR of 108 ± 5 ps FWHM at an energy of 511 keV. Under the same experimental conditions an increase in crystal length to 5 mm deteriorates the CTR to 123 ± 7 ps FWHM, 10 mm to 143 ± 7 ps FWHM and 20 mm to 176 ± 7 ps FWHM. This degradation in CTR is caused by the light transfer efficiency (LTE) and light transfer time spread (LTTS) in the crystal. To quantitatively understand the measured values, we developed a Monte Carlo simulation tool in MATLAB incorporating the timing properties of the photodetector and electronics, the scintillation properties of the crystal and the light transfer within the crystal simulated by SLITRANI. In this work, we show that the predictions of the simulation are in good agreement with the experimental data. We conclude that for longer crystals the deterioration in CTR is mainly caused by the LTE, i.e. the ratio of photons reaching the photodetector to the total amount of photons generated by the scintillation whereas the LTTS influence is partly offset by the gamma absorption in the crystal.

1. Introduction

In a positron emission tomography (PET) system the image quality determined by the signal to noise ratio (SNR) can be drastically improved by using time of flight (TOF) information [1]. This additional time information improves the prior information on the exact localization of the positron emission point and thus contributes to the rejection of background events outside the region of interest, reducing the noise in the reconstructed image and increasing the image contrast. In Fig. 1 the schematic of a whole body PET system can be seen. The radioactive β^+ decay of a biomarker (tracer), e.g. fluorodeoxyglucose (FDG), produces a positron resulting in the emission of two anti-parallel 511 keV gammas by annihilation with an electron. These (nearly) collinear 511 keV photons are detected in opposite detectors (see Fig. 1) and

determine the line of response (LOR) along which the emission took place. Without any time information all points along the LOR have the same probability of being the origin of the β^+ emission, i.e. being emitted by the cancer cells. To determine the exact position of the cancer one needs to overlap the information of many of such decays, commonly done by the Radon transformation. If in addition the time resolution of the detector was sufficient to determine the point of emission of every β^+ decay true 3D image reconstruction based on single events would be possible.

The image SNR gain of a TOF-PET system compared to a non-TOF-PET system can be expressed by Eq. (1), as described in Ref. [1]:

$$G = \frac{SNR_{TOF}}{SNR_{non-TOF}} = \sqrt{\frac{D}{c*CTR}} \qquad (1)$$

The term D denotes the diameter of the volume to be examined, c is the speed of light in vacuum and CTR is the coincidence time resolution achieved by the system. Examples of the gain of a whole

* Corresponding author. Tel.: +41 22 767 4623.
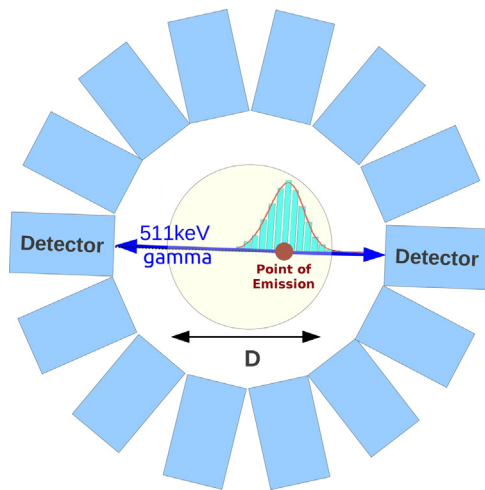 E-mail address: stefan.gundacker@cern.ch (S. Gundacker).

Fig. 1. Schematic of a PET detector ring.

Table 1
Signal to noise ratio gain of a TOF-PET system compared to non-TOF for a whole body PET with $D=40$ cm.

CTR	G
1 ns	1.6
500 ps	2.3
100 ps	5.2

body TOF-PET system ($D=40$ cm) compared to non-TOF are listed in Table 1.

A CTR=100 ps FWHM corresponds to 1.5 cm position resolution and a SNR gain of 5. Thus, for constant image quality, a TOF-PET system with 100 ps CTR can either give a 5 times shorter examination time of the patient or a 5 times lower radiation dose to the patient.

Currently commercial full-body PETs achieve a CTR of ~ 500 ps FWHM [2–4]. More advanced research solutions aim at a CTR of 200 ps FWHM [5], corresponding to a zone of ~ 3 cm around the point of emission, sufficient to remove coincidence events outside the organ of interest. To further improve the CTR towards 100 ps requires detailed studies and knowledge of the full photodetection chain comprising the scintillating crystal, the photodetector and the electronics.

Silicon photomultipliers (SiPMs) or multipixel photon counters (MPPCs) have reached advanced technology maturity and exhibit an excellent time resolution that is promising for the development of new TOF-PET instrumentation [6,7]. In the past we have shown that with 10 mm long crystals, these photodetectors can achieve CTRs of about 200 ps FWHM [8]. These measurements are comparable to and even better than the best values achieved with PMTs [9]. At this high time resolution, the time spread due to photon transport within the crystal turns out to be non-negligible to the overall time resolution [10,11]. Already for crystals with lengths of 3 mm this influence is relatively high, i.e. setting for a $2 \times 2 \times 3$ mm^3 crystal the influence of the photon travel spread (PTS) to zero, would lead to an improvement of 20 ps (from 110 ps FWHM CTR to 90 ps FWHM CTR) [12]. Throughout this work we define the PTS as the combined influence of the gamma interaction point fluctuation in the crystal (given by its absorption characteristics) and the scintillation light transfer time spread (LTTS). The LTTS is the time fluctuation of a scintillation photon from the time of its production to impinging on the photodetector assuming an isotropic angle of emission. Hence the LTTS is dependent on the gamma interaction point (scintillation origin) in the crystal.

This work is organized in three main sections; first we present measurements for different crystal lengths of 3 mm, 5 mm, 10 mm and 20 mm. The second part compares the predicted CTR values of a specially developed Monte Carlo simulation tool with the measurements. And the third part models the different contributions to the time resolution such as light transfer efficiency (LTE) and photon travel spread (PTS).

2. Coincidence time resolution measurement setup

The CTR is measured with a pair of identical crystals and SiPMs in a back-to-back configuration as shown in Fig. 2. We use LSO:Ce codoped 0.4%Ca crystals [13] from the producer Agile with properties similar to those commonly used in PET systems, i.e. being non-hygroscopic and with high gamma detection efficiency per unit length. The crystals have a 2×2 mm^2 cross-section and are coupled to the SiPM (Hamamatsu S10931-050P MPPC) with optical grease Rhodorsil 47 V. We wrapped the scintillators fully in Teflon, except for the side faced to the MPPC. The ultra-fast leading edge discriminator-amplifier NINO [14] gives an output signal if the SiPM signal crosses a defined threshold value, delivering the time information. The dual pulse heights from the voltage amplifier outputs define the energy information. With a high bandwidth oscilloscope, LeCroy DDA 735Zi (40GS/s), we record the dual pulse heights of each branch of the coincidence setup, together with their leading edge delays measured by NINO. In the offline data analysis, we select only events from the two photopeaks, to largely suppress Compton events, and plot the corresponding delay time histogram from which we determine the CTR value with a Gaussian fit [12]. An example of this procedure can be seen in Fig. 3. For these particular plots we used two $2 \times 2 \times 10$ mm^3 LSO:Ce codoped 0.4%Ca crystals.

3. CTR and light output measurements for different crystal lengths

The time resolution and light output were determined for different crystal lengths in the same coincidence configuration as shown in Fig. 2. In Fig. 4 we depict the CTR versus the SiPM bias overvoltage for these different crystal lengths, always measured at a NINO threshold of 80 mV (this is equivalent to approximately half a single MPPC cell amplitude height). A minimum of the CTR as a function of overvoltage can be seen at ~ 2.2 V for all crystal lengths. Examples of delay time histograms with best CTR values achieved are shown in Fig. 5, i.e. for 5 mm and 20 mm lengths. A summary of the measured CTR and corresponding light output values can be seen in Table 2.

We always measured two crystals in coincidence, however with different surface state configurations as can be seen in column two of Table 2. The term "5FP" means that the 2×2 mm^2 face opposite to the SiPM is unpolished, whereas "6FP" denotes that all faces of the crystal are polished. This work mainly aims at the comparison between MC simulation and experimental data. Hence the use of different surface configurations has no problem as long as this circumstance is taken into account in all MC simulations and calculations. The light output values are taken from Ref. [12]. For the 10 mm crystal length configuration we account for the different surface states by averaging the light output value over the 5FP and 6FP cases as for this particular crystal length we used a 5FP versus 6FP configuration in the CTR setup (see Table 2). In addition we want to mention that the LY difference between 5FP and 6FP crystals with same length is small, of the order of a few percent. This further justifies the use of crystals with different surface finishings.

In Fig. 6 we show the best CTR measured versus the crystal length (crystals were wrapped in Teflon and coupled with optical grease to the
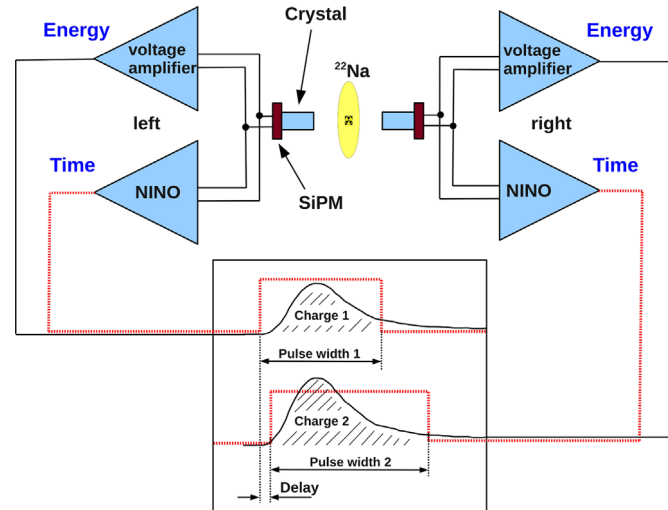
Fig. 2. Schematic of the coincidence setup. Two similar detector configurations are used on both sides. Time information is deduced from the NINO output pulse and energy information from the analog SiPM signal.
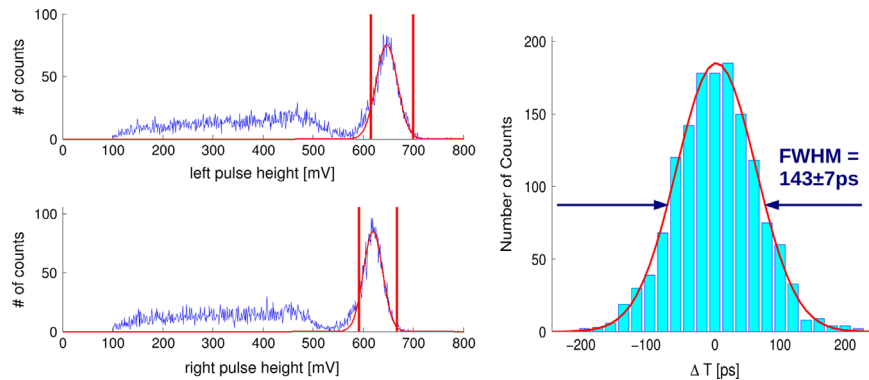

Fig. 3. Typical energy (amplifier output pulse height) spectra and a coincidence delay time histogram of two correlated gammas from ^{22}Na for LSO:Ce codoped Ca with dimensions of $2 \times 2 \times 10$ mm^3, fully wrapped in Teflon and coupled to the SiPM with optical grease Rhodorsil 47 V.
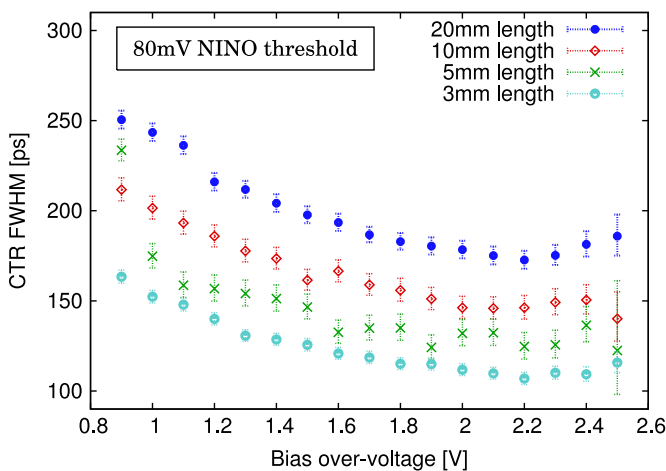

Fig. 4. Measured CTR as a function of SiPM bias overvoltage for different crystal lengths at a NINO threshold of 80 mV. An optimum in CTR can be seen at approximately 2.2 V overvoltage similar for all crystal lengths.

SiPM) and the CTR corrected for the light output as shown in Fig. 7. The light output was measured with a Photonis XP2020Q photomultiplier tube and not with the MPPC itself for the following reason: LY measurements in a SiPM are prone to nonlinearities arising from optical crosstalk, the DCR (dark count rate) and photon pileup due to the limited number of SPADs in the chosen device. These shortcomings are not present in PMTs, notably the Photonis XP2020Q where we applied for the LY only a wavelength-dependent correction to the quantum efficiency. The mentioned CTR correction accounts for the photon statistics and therefore is done with the square root of the relative light output (normalized to the 3 mm case) [15]. Even by applying this correction, an increase in CTR value with crystal length still remains (see Fig. 6). This increase is caused by the LTTS plus the gamma interaction point fluctuation in the crystal. Looking at Fig. 6 we notice that for longer crystals the light output correction has a larger effect and that the deterioration in CTR caused by the PTS seems to level off. This asymptotic behavior can be explained by the gamma interaction probability in the crystal which is highest near the entrance of the crystal and decreases exponentially with an interaction length of ~ 12 mm in LSO [16]. Thus, for long crystals the density of gamma interactions along the crystal axis decreases rapidly making the contribution of gamma interactions close to the photodetector less important. A possible consequence is that for long crystals (>10 mm–20 mm) the LTE begins to dominate the CTR in contrast to the PTS.

4. Monte Carlo simulation framework

To predict the CTR measurements and to get a reliable time model we developed a Monte Carlo (MC) simulation program that includes the light ray tracing simulations from SLITRANI [12]. Fig. 8
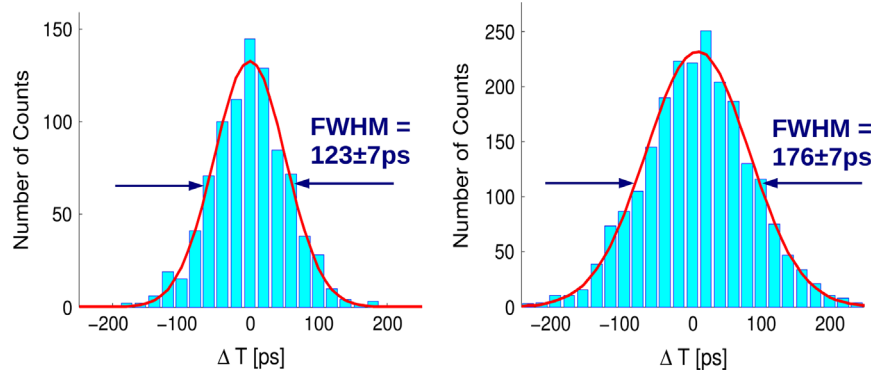
Fig. 5. Measurements for LSO:Ce codoped 0.4%Ca with dimensions of $2 \times 2 \times 5$ mm^3 and $2 \times 2 \times 20$ mm^3 yield a CTR of 123 ± 7 ps and 176 ± 7 ps, respectively.

Table 2
Geometrical properties, CTR configuration, measured light output [12] and measured CTR of the used crystals. The term "5FP" refers to the 2×2 mm^2 face opposite to the SiPM being unpolished. Whereas "6FP" means that all crystal faces are polished. Crystals were fully wrapped in Teflon and coupled to the photodetector with optical grease (Rhodorsil 47 V).

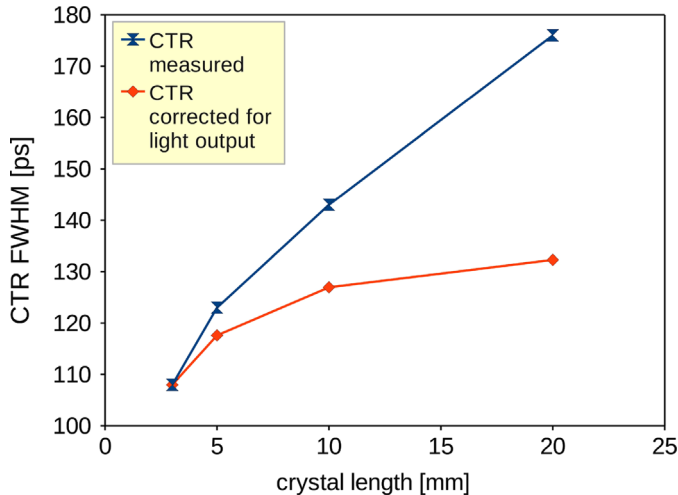| Size (mm^3)	Configuration surface state	Averaged light output (kph/MeV)	CTR (ps)
$2 \times 2 \times 3$	5FPvs5FP	26.2 ± 1.3	108 ± 5
$2 \times 2 \times 5$	5FPvs5FP	24.0 ± 1.2	123 ± 7
$2 \times 2 \times 10$	5FPvs6FP	20.7 ± 1.0	143 ± 7
$2 \times 2 \times 20$	6FPvs6FP	14.8 ± 0.7	176 ± 7

Fig. 6. CTR measured for different crystal lengths and CTR corrected for the light output. The bias overvoltage was set to 2.3 V for the CTR measurements.

Fig. 7. Light output versus crystal length. Measured with a Photonis XP2020Q photo multiplier tube (PMT), values taken from Ref. [12].

Fig. 8. We developed a Monte Carlo (MC) simulation tool in MATLAB modeling the complete sequence of time evolution, i.e. gamma ray conversion, scintillation light production and transport in the crystal (simulated by SLITRANI), extraction and conversion in the SiPM photodetector and electronic readout, taking also into account single photon time resolution (SPTR) and electronic noise. The flow diagram shows the special case of a 3 mm long crystal (5FP).

shows a schematic describing the components taken into account in the Monte Carlo simulation Fig. 8.

In the MC simulation we recorded the time Δt from the generation of the gamma until its absorption in the crystal. At the point of gamma absorption 20 400 photons/511 keV are emitted isotropically [12]. For the utilized LSO:Ce codoped 0.4%Ca crystal the emission of the k-th scintillation photon $t_{Scintillation}(k)$ is modeled by a bi-exponential with a rise time of 70 ps and a fall time of 30 ns [12]. Every k-th scintillation photon is subject to light ray tracing in SLITRANI. With the light ray tracing program we thus calculate the LTTS and the LTE. The LTTS gives rise to a time jitter of every k-th photon which is described by $t_{light\ transfer}$ in Eq. (2). It should be noted that the LTTS and LTE are dependent on the gamma interaction point in the crystal. The timing properties of the photodetector are accounted for by adding an additional time event t_{SPTR} that is Gaussian
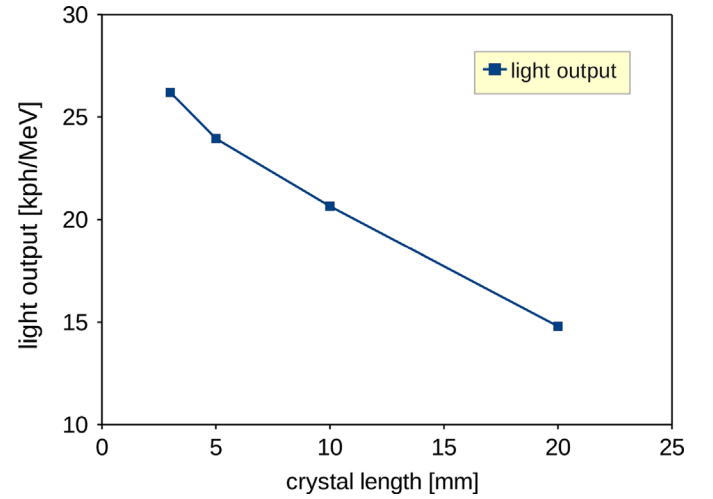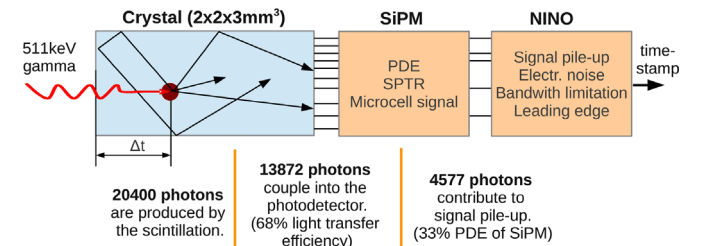
distributed describing the single photon time resolution (SPTR) expressed as standard deviation:

$$t_{k-thphoton} = \Delta t + t_{Scintillation}(k) + t_{light\ transfer} + t_{SPTR} \qquad (2)$$

We then overlap the microcell signal responses of the detected photons with the proper time delay, according to Eq. (2). As can be seen in Fig. 8, detected photons had to undergo absorption in the crystal and detection by the SiPM expressed by the LTE and the photon detection efficiency (PDE), respectively. On the resulting signal we apply leading edge discrimination taking also into account noise and bandwidth limitations of the electronics (see Fig. 9).

A more detailed description and definition of the MC input parameters can be found in Ref. [12] Fig. 9.

5. Comparison of simulations with measurements

In this section we compare the CTR measurements with the Monte Carlo simulations. It should be noted that in our simulation we deduced all MC input parameters from CTR-independent measurements [12] to avoid bias to the calculated CTR values as much as possible.

In Figs. 10–13 we show the measured CTR versus bias overvoltage and CTR versus the NINO threshold. The simulations are plotted as solid lines with their corresponding error "bands". The figures show that our simulation tool is in good agreement with the CTR measurements in terms of the SiPM bias overvoltage and NINO threshold scans. This was already shown in Ref. [12]. The MC
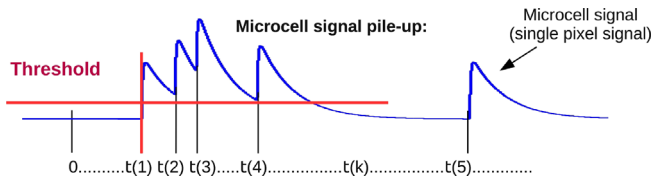
Fig. 9. Illustration of the microcell signal pile-up. Each microcell signal is added with the proper delay resulting from the gamma interaction, scintillation statistics, light transfer time spread and smearing by the single photon time resolution of the detector. Applying a threshold on the summed signal gives the time stamp for one 511 keV gamma. In reality pile-up is so rapid that the subsequent cell-signals already sum up on the rising edge of the first cell-signal.
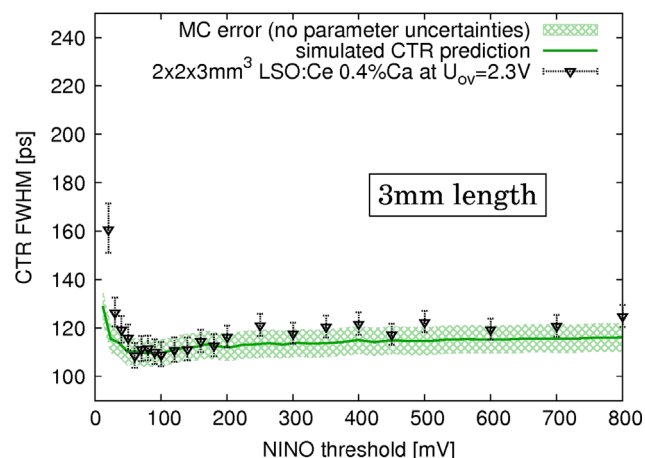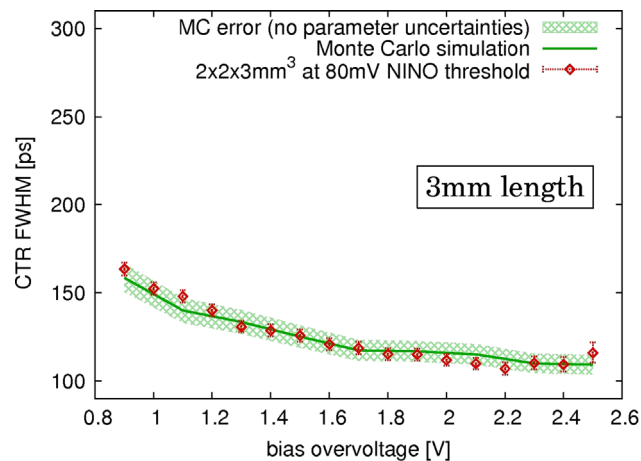
Fig. 10. Measurements for LSO:Ce codoped 0.4%Ca with dimensions of $2 \times 2 \times 3$ mm^3 yielding to a minimum CTR of 108 ± 5 ps.
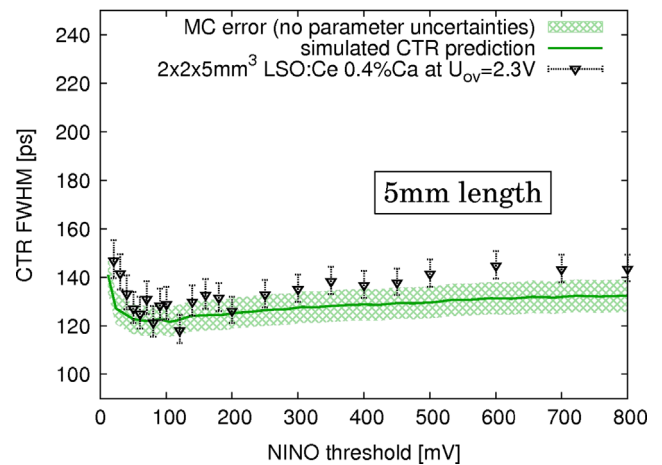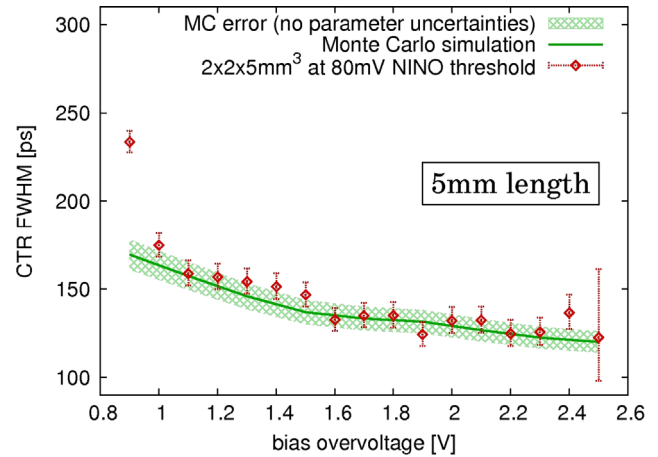
Fig. 11. Measurements for LSO:Ce codoped 0.4%Ca with dimensions of $2 \times 2 \times 5$ mm^3 yielding to a minimum CTR of 123 ± 7 ps.

tool also closely predicts the deterioration of the CTR with increasing crystal length. However, for longer crystals we notice a systematic underestimation of the predicted CTR values as compared to the measurements. This could be a hint that our simulation underrates the LTTS for longer crystals. A possible reason is an additional time smearing caused by random delays of photons scattered by the Teflon reflector. Another explanation could be a poor polished surface state of the lateral faces, which we observed for the 20 mm case. This would cause additional light loss during the transfer and thus explains the observed deviations for the longer crystal cases.

The simulations are able to represent our measurements within the combined errors of the experiment and simulations. The MC simulation error takes into account only the uncertainty due to the limited number of simulated gamma interactions, namely 5000 (purely statistical error). Thus, we have not yet incorporated the uncertainties of the individual input parameters, which would increase the MC error bars by a sizable amount.

6. Discussion

All simulations were performed with an intrinsic light yield of $39\,920 \pm 4000$ ph/MeV, which we determined for our LSO:Ce codoped 0.4%Ca scintillators from the work of Ref. [12]. The deterioration of the CTR values with increasing length is a combined effect of LTE and PTS, as we can describe the SLITRANI light ray tracing results by only these two terms. The MC
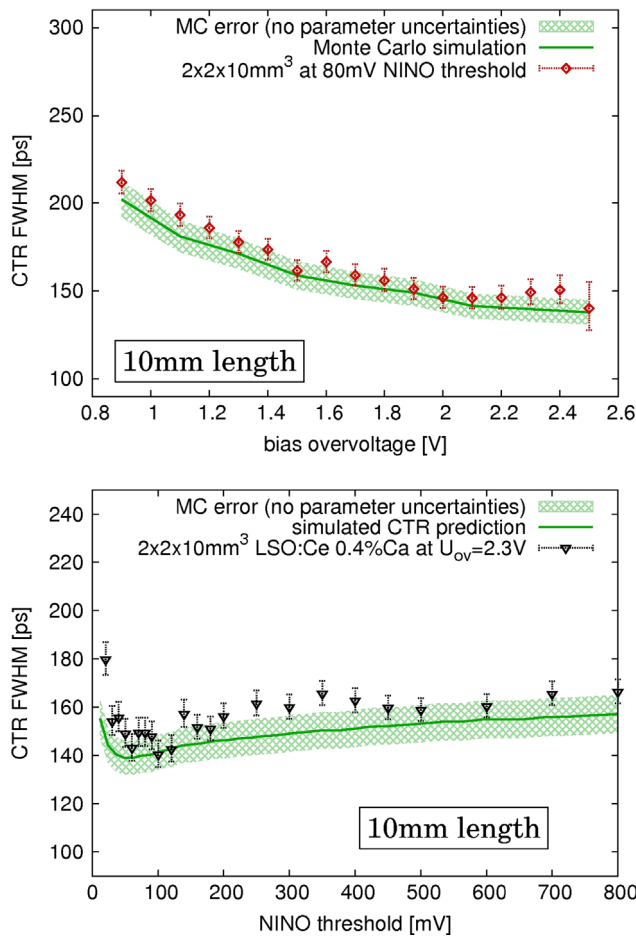
Fig. 12. Measurements for LSO:Ce codoped 0.4%Ca with dimensions of $2 \times 2 \times 10 \text{ mm}^3$ yielding to a minimum CTR of 143 ± 7 ps.

Fig. 13. Measurements for LSO:Ce codoped 0.4%Ca with dimensions of $2 \times 2 \times 20 \text{ mm}^3$ yielding to a minimum CTR of 176 ± 7 ps.

simulation seems to predict the measured CTR very well, justifying to investigate the influence of the LTE and PTS to the CTR in more detail. In Fig. 14 we show the best measured CTR values for different crystal lengths compared with the standard Monte Carlo simulation, i.e. taking all factors into account in order to simulate the measurement setup. As already mentioned the simulation underestimates the CTR values for larger crystal lengths. This behavior is still under investigation but can be an indication that in our simulation we systematically underestimate the LTTS. We also show the CTR versus the crystal length if the LTE is kept constant. Fig. 14 shows two cases, LTE corresponding to the case of $2 \times 2 \times 3 \text{ mm}^3$ size (LTE=0.68) and LTE set to one. These curves demonstrate the influence of the PTS to the overall time resolution. We only see a slight deterioration of the CTR with increasing crystal length, i.e. for LTE=1 from 93 ps at 3 mm to 107 ps at 20 mm. On the other hand, if we set the PTS to zero the degradation in CTR with increasing length is more pronounced, i.e. from 90 ps at 3 mm to 125 ps at 20 mm. Thus, the MC simulation forecasts that for increasing crystal length the PTS contributes less than the LTE. This behavior was already observed in Fig. 6, where we corrected the measured CTR for the measured light output. Although the PTS influence increases only marginally with increasing crystal length its overall influence is noticeable. Turning off the PTS for the $2 \times 2 \times 3 \text{ mm}^3$ size improves the CTR from 110 ps to 90 ps, for the $2 \times 2 \times 20 \text{ mm}^3$ size from 166 ps to 125 ps.

To understand the MC simulation in more detail we show in Figs. 15 and 16 the histogram of the LTTS, the weighted LTTS and the weighted PTS for a $2 \times 2 \times 3 \text{ mm}^3$ and $2 \times 2 \times 20 \text{ mm}^3$ crystal, respectively. The LTTS, shown as solid line, represents the time
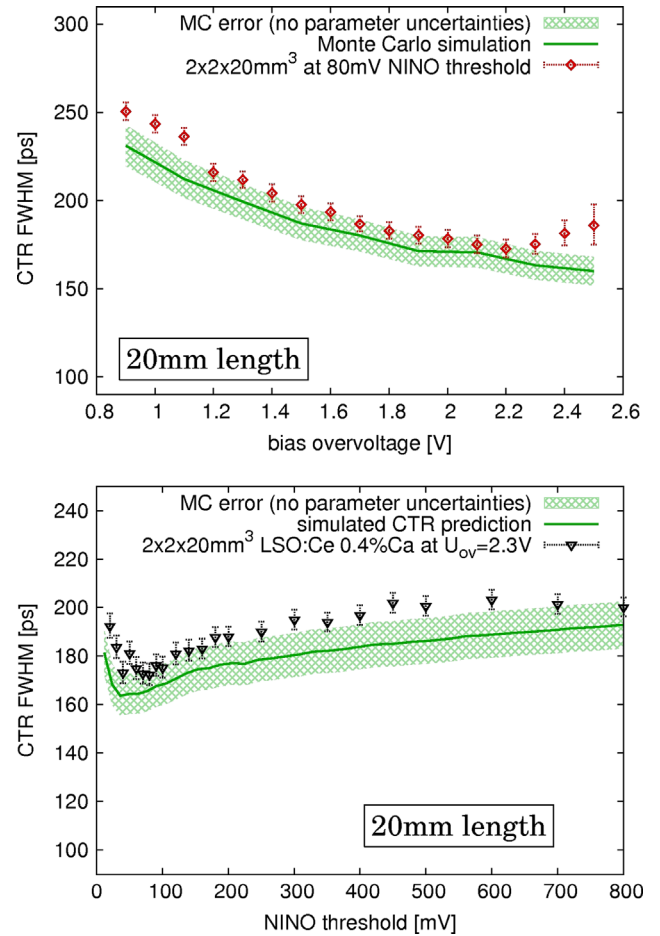
from the emission of a scintillation photon to reach the photo-detector, with equal emission probability at every position in the crystal. In Fig. 15 the LTTS shows two peaks, the first one is caused by photons being emitted towards the SiPM (direct photons) whereas the photons in the second peak had to undergo at least one reflection on the "back" face opposite to the SiPM until reaching the photodetector. The tail seen at larger times is caused by photons that cannot escape the crystal directly and thus are subject to scattering, e.g. in the crystal bulk, at the surface or wrapping. We show as "weighted LTTS" the LTTS weighted by the gamma absorption in the crystal with an absorption length of 12 mm. For longer crystals (see Fig. 16) the weighted LTTS histogram is squeezed in time as compared to the LTTS, which is caused by a higher probability of emission of scintillation photons at the opposite side of the SiPM, where gamma events are being absorbed with a higher probability. If in addition we account for the travel time of the gamma in the crystal we define the weighted PTS. The weighted PTS histogram is even more squeezed in time than the weighted LTTS, giving evidence that the gamma interaction in the crystal is able to offset at least partly the LTTS. This type of offset is only valid if the gamma enters the crystal opposite to the SiPM. Thus, a later conversion of the gamma (deeper penetration into the crystal) entails a shorter distance for scintillating photons directly emitted to the SiPM. Hence, the gamma absorption in the crystal plays an important role in reducing the effect of the scintillation light transfer time spread, becoming more relevant for increasing crystal length.

In Figs. 17 and 18 we show the LTTS as a function of the depth of interaction (DOI) for 3 mm and 20 mm crystal lengths,
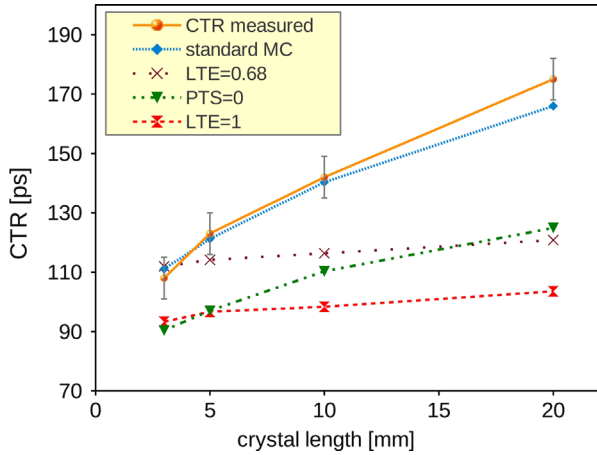
Fig. 14. Measured CTR compared with the standard MC simulation, with simulated constant LTE and zero PTS. If the LTE is held constant at a value of one and equal to that of the 3 mm case (LTE=0.68), only a small deterioration with increasing crystal length is seen. If the PTS is set to zero the deterioration is more pronounced.
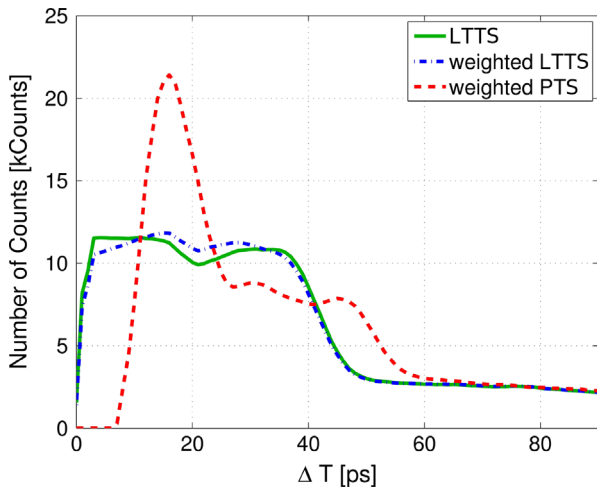
respectively. In Fig. 18, for example (while same arguments also hold for Fig. 17), three different DOI configurations for a 20 mm long crystal are shown. DOI=20 mm denotes a gamma interaction taking place in a $2 \times 2 \times 0.5$ mm^3 slice adjacent to the SiPM. Two light peaks can be seen, a first one at 0 ps stemming from photons emitted directly to the SiPM and a second peak at 280 ps originating from photons emitted to the other side of the crystal and thus reflected at the crystal surface opposite to the SiPM. DOI=0 mm, on the other hand, describes the case where the gamma interaction was at the entrance face of the crystal, i.e. opposite to the SiPM. Consequently both the reflected and direct photons need approximately the same time to reach the photo-detector. This then shows up as a single peak in both figures.

If for a 20 mm long crystal the gamma interaction takes place close to the SiPM (DOI=20 mm), the back-reflected photons undergo a large delay of ~ 280 ps as can be seen in Fig. 18. Whether these delayed photons contribute to the CTR or not will be explained as follows: in the MC simulation for the $2 \times 2 \times 20$ mm^3 crystal we force the gamma interactions to be close to the SiPM (DOI=20 mm), i.e. in a $2 \times 2 \times 1.5$ mm^3 slice adjacent to the SiPM. In this specially prepared simulation we estimate the average time lag from the instant of gamma conversion to the point of reaching the highest CTR to ~ 250 ps. Therefore, combining the results in Fig. 18

Fig. 15. Histogram of LTTS, weighted LTTS and weighted PTS for a $2 \times 2 \times 3$ mm^3 crystal. Weighted LTTS accounts for the absorption length of the gamma photon and weighted PTS in addition to the travel time of the gamma in the crystal.
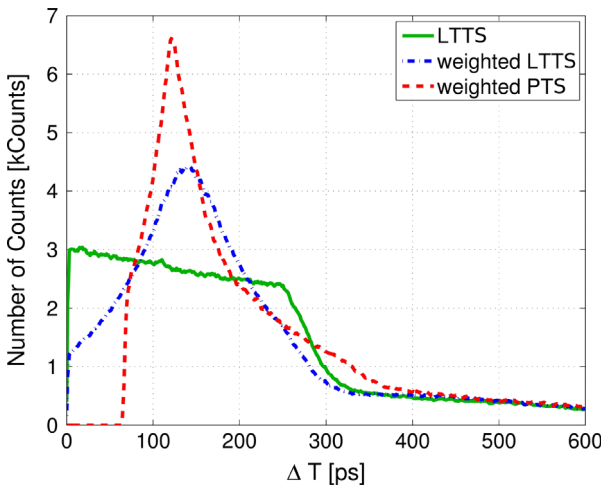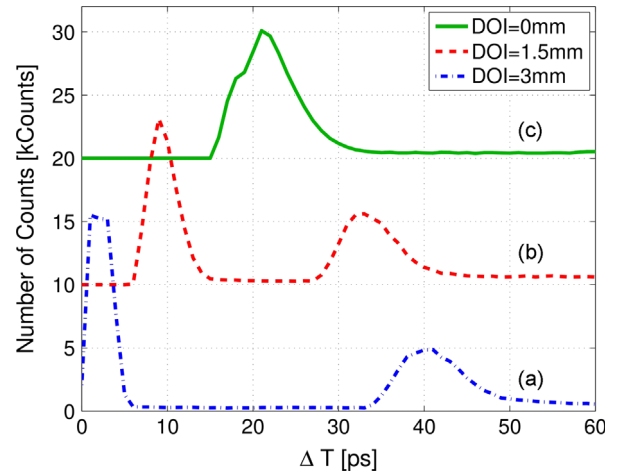

Fig. 17. LTTS at fixed DOI for a 3 mm long crystal: (a) gamma interaction near the SiPM (DOI=3 mm), (b) in the middle of the crystal (DOI=1.5 mm) and (c) opposite to the SiPM near the crystal surface (DOI=0 mm).

Fig. 16. Histogram of LTTS, weighted LTTS and weighted PTS for a $2 \times 2 \times 20$ mm^3 crystal. Weighted LTTS accounts for the absorption length of the gamma photon and weighted PTS in addition to the travel time of the gamma in the crystal.
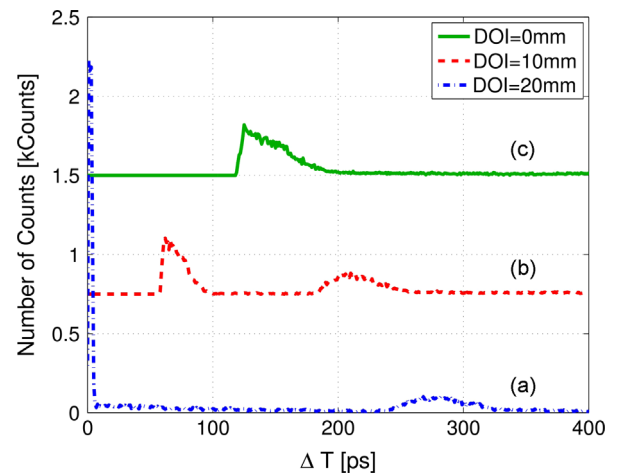

Fig. 18. LTTS at fixed DOI for a 20 mm long crystal: (a) gamma interaction near the SiPM (DOI=20 mm), (b) in the middle of the crystal (DOI=10 mm) and (c) opposite to the SiPM near the crystal surface (DOI=0 mm).

Table 3
Simulated coincidence time resolution as a function of the crystal cross-section. The active area of the SiPM is 3×3 mm^2. Crystals have a length of 20mm, are wrapped in Teflon and polished on all sides.

Scintillator cross-section (mm^2)	LTE (%)	CTR (ps)
0.5×0.5	29	176 ± 9
1×1	34	166 ± 8
2×2	37	165 ± 8
3×3	32	178 ± 9

(DOI=20 mm) with this outcome shows that reflected photons from a 20 mm long crystal simply arrive too late at the photodetector to contribute to the CTR that had already reached its optimum value ~ 30 ps prior from the directly emitted photons. This fact would also explain why in longer crystals the LTTS has less influence on the CTR with increasing crystal length.

To investigate the influence of the crystal cross-section to the CTR we simulated different configurations as shown in Table 3. In this simulation we kept the SiPM's active area constant at 3×3 mm^2 and varied only the crystals' cross-section of a 20 mm long crystal from 0.5×0.5 mm^2 to 3×3 mm^2. As the results show, the simulated CTR does not change significantly as a function of the chosen crystal cross-sections. Small deteriorations in CTR can only be seen for 0.5×0.5 mm^2 and 3×3 mm^2 sections. For the 0.5×0.5 mm^2 case the absorption of scintillation light increases (expressed by a lower LTE) due to an increase in the number of reflections from the Teflon shield, giving rise to a slight deterioration in CTR. On the other hand in crystals with 3×3 mm^2 cross-section, a small loss in scintillation light and thus in photostatistics is caused by photons that may escape through the sidewalls of the 0.5 mm thick silicon resin layer protecting the SiPM surface. We therefore conclude that the crystals cross-section plays only an inferior role in the achievable timing performance, which is supported by measurements presented in Ref. [10] Table 3.

7. Conclusion

In a TOF-PET system a crystal length of 20 mm or longer is necessary to achieve adequate detection efficiency for the 511 keV gammas. Measurements were performed using NINO for the leading edge time information and an analog amplifier for the energy information. We achieve CTR values of 108 ps FWHM for $2 \times 2 \times 3$ mm^3, 123 ps FWHM for $2 \times 2 \times 5$ mm^3, 143 ps FWHM for $2 \times 2 \times 10$ mm^3 and 176 ps FWHM for $2 \times 2 \times 20$ mm^3 LSO:Ce codoped 0.4%Ca crystals. Correcting the measured CTR for the measured light output of the crystal with various lengths we could show that the influence of the photon travel spread (PTS) levels off with increasing length. We identified three mechanisms responsible for this behavior (a) the absorption of the gamma in the crystal with its characteristic absorption length of 12 mm reducing the effective sampling of the crystal, (b) the time delay of the gamma entering the crystal until being absorbed, which acts as an offset to the light transfer time spread (LTTS) and (c) highly delayed scintillation photons (e.g. back-reflected photons) that will likely not contribute to the time stamp derived from photo-electron pile-up with leading edge discrimination.

To analyze the measurements in more detail we developed a Monte Carlo simulation tool dedicated to model the complete chain from the gamma ray conversion, scintillation light production and transport in the crystal, light extraction and conversion in the SiPM photodetector to the electronic readout, taking also into account single photon time resolution (SPTR), electronic noise and bandwidth limitations of the electronics. The MC simulation predicts and matches well the measured CTR values as a function of SiPM bias overvoltage and NINO threshold. In addition, the MC tool is also able to affirm the deterioration of the CTR with increasing crystal length. From the simulation it appears that the PTS plays an inferior role to the CTR with increasing crystal length than the light transfer efficiency (LTE), which is in good agreement with the measurements (see Fig. 6). Despite the fact that in our simulation the PTS does not increase significantly with increasing length, its overall influence still seems to be quite high. If in the simulation we "turn off" the PTS contribution for the $2 \times 2 \times 3$ mm^3 crystal size the CTR would improve from 110 ps to 90 ps and for the $2 \times 2 \times 20$ mm^3 size from 166 ps to 125 ps. Setting, in contrast to the above, the LTE in our simulation to one would improve the CTR from 110 ps to 93 ps for a $2 \times 2 \times 3$ mm^3 sized crystal and from 166 ps to 104 ps for a $2 \times 2 \times 20$ mm^3 sized crystal. It should be noted that the latter improvement (from 166 ps to 104 ps) is most likely overestimated since our simulation systematically underestimates the LTTS for longer crystals, e.g. the 20 mm case.

Our MC simulation also comprised an investigation of the influence of crystal cross-section on CTR. Within the framework of the studied cases, shown in Section 6, and in agreement with Ref. [10], the CTR changes only insignificantly with respect to the scintillator cross-section.

To achieve a CTR of 100 ps FWHM using crystals with lengths necessary for TOF-PET systems, i.e. 15–30 mm, one has to account for both the LTE and PTS. The scintillation light transfer in the crystal has to be understood in more detail, in particular the influence of wrapping. Also a better extraction of the scintillation light into the photodetector must be achieved. Photonic crystals are an interesting approach to meet this challenge [17]. Concepts of employing a double sided readout of the crystal that incorporates the depth of interaction information is also expected to improve the CTR.

References

[1] M. Conti, Phys. Med. 25 (2009) 1–11.
[2] B.W. Jakoby, Y. Bercier, M. Conti, M.E. Casey, B. Bendriem, D.W. Townsend, Phys. Med. Biol. 56 (April 8) (2011) 2375.
[3] V. Bettinardi, L. Presotto, E. Rapisarda, M. Picchio, L. Gianolli, M.C. Gilardi, Med. Phys. 38 (10) (2011) 5394.
[4] S. Surti, A. Kuhn, M.E. Werner, A.E. Perkins, J. Kolthammer, J.S. Karp, J. Nucl. Med. 48 (March (3)) (2007) 471.
[5] B. Frisch, on behalf of the EndoTOFPET-US Collaboration, Combining endoscopic ultrasound with Time-Of-Flight PET: The EndoTOFPET-US Project, Nucl. Instrum. Methods Phys. Res. A (2013) 732 (2013) 577–580, http://dx.doi.org/10.1016/j.nima.2013.05.027).
[6] C.L. Kim, G.C. Wang, S. Dolinsky, IEEE Trans. Nucl. Sci. NS-56 (October (5)) (2009) 2580.
[7] R. Vinke, H. Lohner, D.R. Schaart, H.T. van Dam, S. Seifert, F.J. Beekman, P. Dendooven, Nucl. Instrum. Methods Phys. Res. A 610 (2009) 188.
[8] S. Gundacker, E. Auffray, B. Frisch, H. Hillemanns, P. Jarron, T. Meyer, K. Pauwels, P. Lecoq, IEEE Trans. Nucl. Sci. NS-59 (October (5)) (2012) 1798.
[9] T. Szczesniak, M. Moszynski, L. Swiderski, A. Nassalski, P. Lavoute, M. Kapusta, IEEE Trans. Nucl. Sci. NS-56 (February (1)) (2009) 173.
[10] E. Auffray, B. Frisch, F. Geraci, A. Ghezzi, S. Gundacker, H. Hillemanns, P. Jaron, T. Meyer, M. Paganoni, K. Pauwels, M. Pizzichemi, P. Lecoq, A comprehensive and systematic study of coincidence time resolution and light yield using scintillators of different size, wrapping and doping NSS/MIC, in: 2011 IEEE, Valencia, 23–29 October 2011, pp. 64–71.
[11] W.W. Moses, S.E. Derenzo, IEEE Trans. Nucl. Sci. NS-46 (1999) 474.

[12] S. Gundacker, E. Auffray, B. Frisch, P. Jarron, A. Knapitsch, T. Meyer, M. Pizzichemi, P. Lecoq, J. Instrum. 8 (2013) P07014, http://dx.doi.org/10.1088/1748-0221/8/07/P07014.

[13] M.A. Spurrier, P. Szupryczynski, K. Yany, A.A. Carey, C.L. Melcher, IEEE Trans. Nucl. Sci. NS-55 (June (3)) (2008) 1178.

[14] F. Anghinolfi, P. Jarron, F. Krummenacher, E. Usenko, M.C.S. Williams, IEEE Trans. Nucl. Sci. 51 (October (5)) (2004) 1974.

[15] L.G. Hyman, R.M. Schwarcz, R.A. Schluter, Rev. Sci. Instrum. 35 (3) (1964) 393.

[16] M.J. Berger, J.H. Hubbell, S.M. Seltzer, J. Chang, J.S. Coursey, R. Sukumar, D.S. Zucker, K. Olsen, Photon Cross Section Database, URL: ⟨http://www.nist.gov/pml/data/xcom/index.cfm⟩.

[17] A. Knapitsch, E. Auffray, C.W. Fabjan, J.L. Leclercq, X. Letartre, R. Mazurczyk, Paul Lecoq, IEEE Trans. Nucl. Sci. NS-59 (October (5)) (2012) 2334.